Kondo Memory in Driven Strongly Correlated Quantum Dots

Xiao Zheng,[1] YiJing Yan,[1,2] and Massimiliano Di Ventra[3]

[1]*Hefei National Laboratory for Physical Sciences at the Microscale, University of Science and Technology of China, Hefei, Anhui 230026, China*

[2]*Department of Chemistry, Hong Kong University of Science and Technology, Kowloon, Hong Kong, China*

[3]*Department of Physics, University of California, San Diego, La Jolla, California 92093, USA*

(Received 7 April 2013; published 19 August 2013)

We investigate the real-time current response of strongly correlated quantum dot systems under sinusoidal driving voltages. By means of an accurate hierarchical equations of motion approach, we demonstrate the presence of prominent memory effects induced by the Kondo resonance on the real-time current response. These memory effects appear as distinctive hysteresis line shapes and self-crossing features in the dynamic current-voltage characteristics, with concomitant excitation of odd-number overtones. They emerge as a cooperative effect of quantum coherence—due to inductive behavior—and electron correlations—due to the Kondo resonance. We also show the suppression of memory effects and the transition to classical behavior as a function of temperature. All these phenomena can be observed in experiments and may lead to novel quantum memory applications.

DOI: 10.1103/PhysRevLett.111.086601 PACS numbers: 72.15.Qm, 73.63.−b, 85.35.Be

The memory of physical systems is quite a common phenomenon [1]. It simply means that the state of a system at a given time—driven by an external input—depends strongly on its history, at least within a certain range of parameters of the external drive, such as its frequency or amplitude [1,2]. These memory features give rise to unconventional properties and novel functionalities that can be used in actual device applications.

Although there has been a recent crescendo of interest in memory effects in resistive, capacitive, and inductive systems [3], less work has been devoted to memory effects in strongly correlated quantum systems. These include the single-molecule magnets [4,5], metal-oxide-semiconductor thin films [6,7], nanoparticle assemblies [8], and bulk Kondo insulators [9]. In this respect, quantum dots (QDs) coupled to electron reservoirs are ideal platforms for experimental and theoretical studies relevant to quantum computation and quantum information [10,11]. This is because the electron or spin state of a QD can be manipulated conveniently by external fields, with the quantum coherence largely preserved. In particular, at low temperatures, formation of the Kondo singlet state [12–15] opens up additional channels for electron conduction. However, it is not at all obvious if new features would emerge due to the interplay between quantum coherence and electron correlations under driving conditions, and if the Kondo phenomena would influence significantly the memory of the QD system.

In this Letter, we show that Kondo resonances indeed induce prominent memory effects when a QD is driven by an external periodic voltage. These features appear as well-defined hysteresis line shapes and self-crossing features in the dynamic current-voltage characteristics with excitation of odd-number overtones. They are a direct consequence of quantum coherence and Kondo correlations, and are suppressed at relatively high temperatures where a classical behavior is recovered.

The QD system of interest is illustrated with a single-impurity Anderson model [16] $H_{\rm dot} = \epsilon_d(\hat{n}_\uparrow + \hat{n}_\downarrow) + U\hat{n}_\uparrow\hat{n}_\downarrow$. Here, $\hat{n}_s = \hat{a}_s^\dagger\hat{a}_s$, and $\hat{a}_s^\dagger$ ($\hat{a}_s$) creates (annihilates) a spin-s electron on the dot level of energy ϵ_d, while U is the on-dot electron-electron (e-e) interaction strength. The total Hamiltonian is

$$H = H_{\rm dot} + H_{\rm res} + H_{\rm coupling}, \tag{1}$$

with $H_{\rm res} = \sum_{\alpha k}\epsilon_{\alpha k}d_{\alpha k}^\dagger d_{\alpha k}$ and $H_{\rm coupling} = \sum_{\alpha k}t_{\alpha k}a_s^\dagger d_{\alpha k} +$ H.c., for the noninteracting leads and the dot-lead couplings, respectively. Here, $d_{\alpha k}^\dagger$ ($d_{\alpha k}$) is the creation (annihilation) operator for the α-lead state $|k\rangle$ of energy $\epsilon_{\alpha k}$, and $t_{\alpha k}$ is the coupling strength between the dot level and $|k\rangle$. For numerical convenience, identical leads are considered, and their hybridization functions assume a Lorentzian form $\Delta_\alpha(\omega) \equiv \pi\sum_k t_{\alpha k}t_{\alpha k}^*\delta(\omega-\epsilon_{\alpha k}) = \Delta W^2/[(\omega-\mu_\alpha)^2+W^2]$, where Δ is the effective dot-lead coupling strength, W is the bandwidth, and μ_α is the chemical potential of the α lead. We prepare the initial total system at equilibrium, where $\mu_\alpha = \mu^{\rm eq} \equiv 0$. An ac voltage is applied to the left (L) and right (R) leads from the time $t_0 \equiv 0$, i.e., $V_L(t) = -V_R(t) = V_0\sin(\Omega t)$, with V_0 and Ω being the voltage amplitude and frequency, respectively. Upon switching on the voltage, the QD is driven out of equilibrium, and the time-dependent current flowing into the α lead $\bar{I}_\alpha(t)$ is computed.

Kondo effects in QDs out of equilibrium have been studied extensively [17–23]. A number of theoretical approaches have been developed [24]. These include a variety of renormalization group approaches [25–36], the real-time and imaginary-time quantum Monte Carlo

 © 2013 American Physical Society

approaches [37–44], the iterative summation of real-time path integrals [45,46], the time-dependent Green's function approach [47,48], the time-dependent density-functional theory [49], and the quantum master equations [5,50–52].

To proceed, we choose the hierarchical equations of motion (HEOM) approach, developed in recent years by Yan and co-workers [53–55]. This is a unified, real-time approach for a wide range of equilibrium and nonequilibrium, static and dynamic properties of a general open quantum system [55–58]. It has been used to study, for instance, the dynamic Coulomb blockade and dynamic Kondo phenomena in QDs [59,60]. To close the coupled equations, the hierarchy needs to be truncated at a certain level L. In principle, the exact solution is guaranteed for $L \rightarrow \infty$. In practice, the results usually converge rapidly with increasing L at finite temperatures. Once the convergence is achieved, the numerical outcome is considered to be quantitatively accurate [55]. It has reproduced [56] the exact numerical solution for the time-dependent current response of a noninteracting QD to a step-function voltage [61,62]. Here, we solve the HEOM dynamics of Hamiltonian (1) at the $L = 4$ truncation level of hierarchy [59,60]. We have checked that all results presented converge quantitatively with respect to this truncation [63].

Figure 1 depicts the dynamic I-V characteristics of a QD with the electron-hole symmetry ($U = -2\epsilon_d$) subject to an ac voltage of various frequencies Ω. To compare with the energetic parameters of the QD, Ω is represented by the harmonic energy of the driving voltage. In particular, $\Omega = 0.01$ meV corresponds to a period of 0.4 ns.

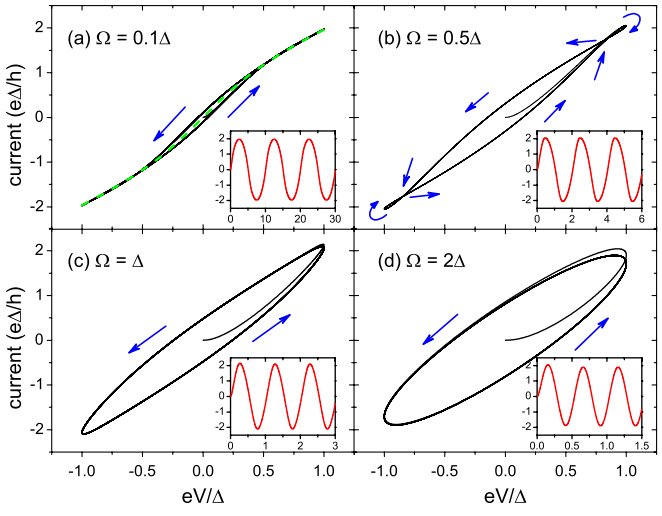

FIG. 1 (color online). Current versus voltage for a QD driven by an ac voltage of amplitude $eV_0 = \Delta$ and frequency Ω. The arrows indicate the circulating directions of the loops. The dashed green curve in (a) depicts the steady-state I–V characteristics. The insets plot the corresponding current (in $e\Delta/h$) versus time (in h/Δ). The other parameters are $U = -2\epsilon_d = 4\Delta$, $W = 20\Delta$, and $T = 0.2\Delta$.

Although high, these GHz time-domain voltage manipulations and current measurements have been realized experimentally [64–66]. The calculation results indicate that the electron-hole symmetry is preserved under the ac voltage, and the dot level is always half-filled. Consequently, the displacement current is zero, and the Kirchhoff's current law holds at any time, i.e., $I(t) = \bar{I}_R(t) = -\bar{I}_L(t)$ [5].

As shown in Fig. 1(a), at a low Ω, the dynamic I-V characteristics are close to the steady-state curve, since the electrons have sufficient time to redistribute to catch up with the variation of voltage. In contrast, at a high Ω, the dynamic I-V curve forms an ellipse; see Fig. 1(d). The ellipse shape originates from a phase difference between the current and voltage. In the case of Fig. 1(d), the ellipse is traversed in the counterclockwise direction (voltage leads current), indicating a prominent inductive behavior. It has been demonstrated that in the linear response regime, a two-terminal device can be mapped onto a classical circuit, where a resistor-capacitor branch and a resistor-inductor branch are connected in parallel [67–69]. The inductance is associated with the time that an electron dwells on the device which is proportional to $1/\Delta$ [67,70] and is due to the fact that the dot energy is lower than the equilibrium energy, as required to have a Kondo resonance. At an intermediate Ω, the dynamic I-V curve forms a hysteresis loop with self-crossing in the first and third quadrants; see Fig. 1(b). The hysteresis behavior highlights the nontrivial memory effects on the real-time electron dynamics. To understand these memory effects, we vary both the level energy ϵ_d and the temperature T.

Figure 2 depicts the dynamic I-V curves for QDs of $\epsilon_d = -U/2 = -2\Delta$, -6Δ, and -10Δ, where the Kondo temperature $T_K = (U\Delta/2)^{1/2}\exp[-\pi U/8\Delta + \pi\Delta/2U]$ are 0.44Δ, 0.025Δ, and 0.0013Δ, respectively. Under the same ac voltage, the hysteresis behavior of Fig. 1(b) is present in all the three QDs, and it is most pronounced at $\epsilon_d = -6\Delta$.

Comparing T_K to $T = 0.1\Delta$, the Kondo resonance is expected to be strongly suppressed and almost vanishing as ϵ_d lowers from -2Δ to -10Δ. This is confirmed by the equilibrium spectral functions $A^{\rm eq}(\omega)$ displayed in the inset of Fig. 2(b), where the Kondo peak height at $\omega = \mu^{\rm eq} = 0$ reduces drastically with decreasing ϵ_d. Kondo effects are further suppressed by bias voltage. The QD spectral function under a stationary voltage $V_L = -V_R = V$, $A(\omega; V)$, is shown in the inset of Fig. 2(c) for $\epsilon_d = -6\Delta$. The Kondo peaks are split by the voltage and locate at $\omega = \pm eV$. The peak height reduces continuously with increasing V. This is in agreement with what has been found by Kaminski *et al.* [71,72], who showed that the suppression of Kondo effects depends universally on the ac field through its strength V_0/T_K and frequency Ω/T_K. In the case of ac gate voltages, the suppression is stronger with an increase of either V_0 or Ω. Instead, under ac bias voltages, the suppression is weak at any Ω for $eV_0 \ll T_K$, while it

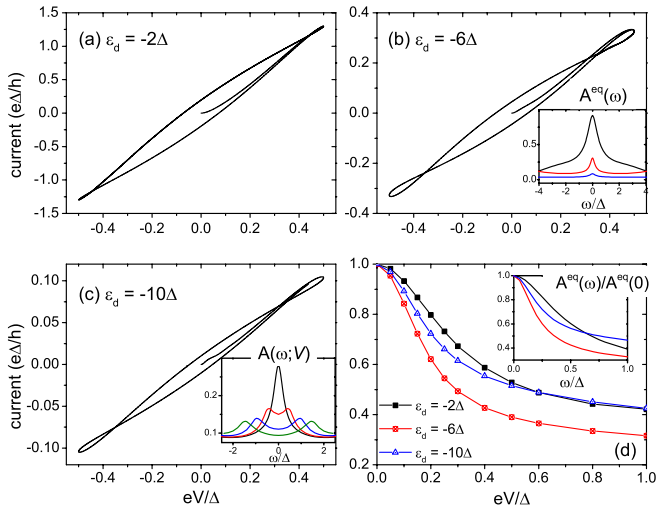

FIG. 2 (color online). (a)–(c) Current versus voltage for QDs of $\epsilon_d = -U/2 = -2\Delta$, -6Δ, and -10Δ, under the ac bias voltage of $eV_0 = 0.5\Delta$ and $\Omega = 0.3\Delta$, and at $T = 0.1\Delta$. The inset of (b) shows $A^{eq}(\omega)$ for $\epsilon_d = -2\Delta$, -6Δ, and -10Δ from up to down. The inset of (c) plots $A(\omega; V)$ under stationary voltages of $eV = 0.1\Delta$, 0.5Δ, Δ, and 1.5Δ from up to down at $\omega = 0$, for the QD of $\epsilon_d = -6\Delta$. (d) Steady-state dI/dV versus the stationary voltage of $V = V_L = -V_R$, where the data are scaled by their values at $V = 0$. The inset shows the corresponding $A^{eq}(\omega)/A^{eq}(0)$.

becomes stronger as Ω decreases for $eV_0 \gg T_K$ [72]. However, although Kondo effects are strongly suppressed by thermal fluctuations and voltage amplitudes, a residual amount of Kondo resonance survives, which gives rise to the quasiparticle peaks at $\omega = \mu_\alpha$. In addition, the ac bias voltage suppresses the Kondo resonance through decoherence of the dot spin. Such a decoherence rate has been found to decrease with increasing Ω [72]. Therefore, the frequencies considered in this Letter only weakly suppress the Kondo resonance.

We then calculate the differential conductance (dI/dV) as a function of stationary bias voltage V. The dI/dV are scaled by their values at $V = 0$ and depicted in Fig. 2(d). For comparison, the corresponding $A^{eq}(\omega)/A^{eq}(\omega = 0)$ are shown in the inset, whose line shapes agree remarkably well with the dI/dV-V lines. They both exhibit a decrease with a slope that is steepest (flattest) at $\epsilon_d = -6\Delta$ (-2Δ). Clearly, both the peaks of dI/dV at $V = 0$ and $A^{eq}(\omega)$ at $\omega = 0$ originate from the Kondo resonance, and their sharpness determines directly the hysteresis behavior. This is true even when there exists only a residual amount of Kondo resonance, for instance, in the case of $\epsilon_d = -10\Delta$.

The shape of the dynamic I-V characteristics can now be interpreted as follows. In the limit of adiabatic driving ($\Omega \to 0$), the evolution of the current response follows exactly the steady-state dI/dV-V curve. The reduction in dI/dV versus V leads to a concave I-V curve at $V > 0$; see the dashed green curve in Fig. 1(a). At a finite Ω, the inductive feature starts to emerge, which forces the current to lag behind the driving voltage. For instance, at an instant when the voltage turns from negative to positive, the current has not yet reached its turning point—it remains negative but accelerates toward the voltage. Consequently, the dynamic I-V curve has a convex curvature at $V = 0$ and $I < 0$. The convexity may be inverted into concavity, provided that the increase in voltage captures the drastic decay in conductance. This requires a relatively low Ω, with which the variation of "transient" conductance does not deviate much from the steady-state dI/dV-V curve shown in Fig. 2(d). Such a convex-concave curve segment, together with its mirror-image counterpart upon voltage decrease, results in a self-crossing hysteresis loop, as depicted in Figs. 1(d) and 2(a)–2(c). At a high Ω, the inductive feature becomes dominant, which effectively smooths the dI/dV-V curve, leading to a simple ellipse shape of the dynamic I–V curve; see Fig. 1(d). To summarize, the hysteresis feature requires Ω to be sufficiently low to have the QD experience the significant variation of conductance and meanwhile high enough to create an appropriate phase difference between the current and voltage.

Based on the above analysis, we can conclude that the hysteresis behavior of the ac I-V characteristics originates from a cooperative interplay between the quantum coherence (the inductive feature) and strong electron correlation (the Kondo resonance). Since both quantum coherence and correlation are significantly influenced by thermal fluctuations, the associated memory effects are expected to depend sensitively on the temperature.

Figure 3(a) shows the evolution of a dynamic I-V curve with the increasing T. Here, to accentuate the nonlinear current response, a somewhat larger voltage amplitude ($eV_0 = \Delta$) is adopted. At the low $T = 0.1\Delta$, the ac I-V curve displays a remarkable hysteresis behavior, with the emergence of multiple self-crossing points. Such a convoluted line shape is a strong indication of complex memory effects. With T raised by as little as 0.1Δ, the hysteresis behavior of Fig. 2(b) is recovered, with only one crossing in the first or third quadrant. This apparent change in the hysteresis pattern is due to the suppression of Kondo resonance by thermal fluctuations. Indeed, as shown in Fig. 3(c), the zero-bias conductance reduces drastically with a minor increase in T from 0.1Δ. Meanwhile, increasing T leads to the progressive narrowing of the I-V hysteresis loop, and the loop almost merges into a single line at $T = \Delta$. This means that the inductive feature becomes irrelevant at a high T, and the QD behaves like a classical resistor. This is because the conducting electrons have a wide energy distribution due to thermal excitations, and the phase difference between the current and voltage is largely randomized. For the same reason, the steady-state dI/dV varies smoothly versus V at a high T, leading to an overall Ohmic conductance.

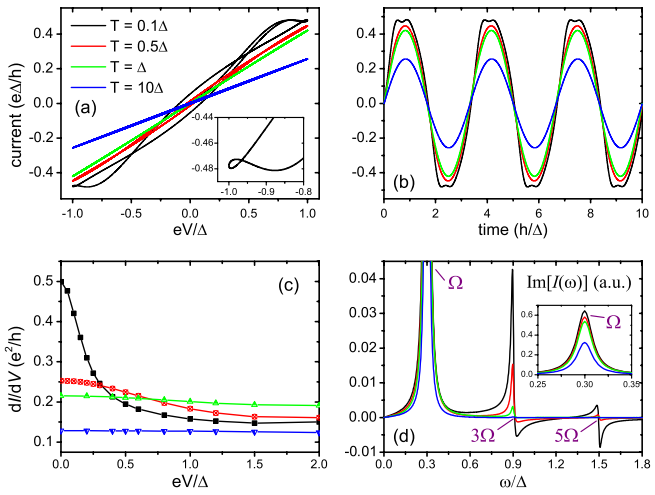

FIG. 3 (color online). (a) Dynamic I-V characteristics, (b) real-time current response, (c) steady-state dI/dV versus V, and (d) imaginary part of the current spectrum of a QD with $U = -2\epsilon_d = 12\Delta$ at various T. The inset of (a) magnifies the self-crossing of the ac I-V curve near $V = -V_0$ at $T = 0.1\Delta$, and that of (b) displays the full peaks of $\mathrm{Im}[I(\omega)]$ at $\omega = \Omega$. The other parameters are $W = 20\Delta$, $eV_0 = \Delta$, and $\Omega = 0.3\Delta$.

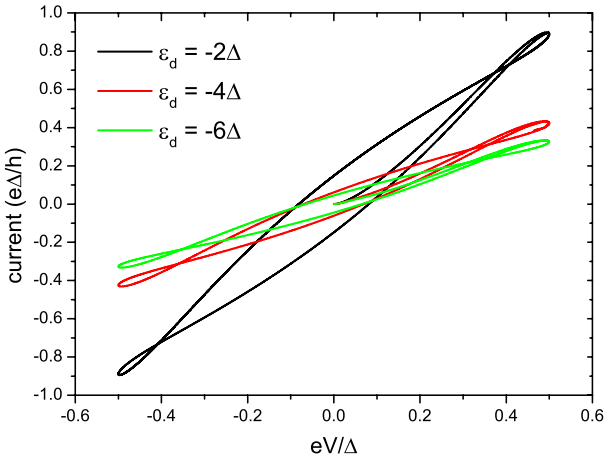

FIG. 4 (color online). Dynamic I-V characteristics of QDs of various ϵ_d. The displayed current is $I(t) = [\bar{I}_R(t) - \bar{I}_L(t)]/2$. The other parameters are $U = 12\Delta$, $T = 0.1\Delta$, $W = 20\Delta$, $eV_0 = 0.5\Delta$, and $\Omega = 0.3\Delta$.

The temperature-sensitive memory is further explored through a frequency analysis of response current. It has been found that the current response of single-lead QDs to sinusoidal voltages concentrates on the exact multiples of driving frequency Ω [68]. For the two-terminal QD studied here, the variation of current spectrum versus temperature is depicted in Fig. 3(d). The response current arises predominantly at $\omega = (2n + 1)\Omega$ with $n \in \mathbb{Z}$, while the even overtones remain unexcited. This is because the ac voltages have the left-right antisymmetry. The response current would flow in the reverse direction if the half-period were taken as the initial time ($t_0 = \pi/\Omega$). Therefore, the relation $I(\omega) = -I(\omega)e^{i\omega\pi/\Omega}$ must be satisfied. Overtones of all symmetries can be found by breaking the symmetric coupling between the QD and the leads [73]. As T rises from 0.1Δ to Δ, the change in current amplitude at the fundamental frequency is rather minor. In contrast, the overtone responses vanish almost completely. This highlights the dynamic Kondo-assisted electron conduction, which requires a relatively low excitation energy. At $T < 0.1\Delta$, the Kondo memory effects are expected to be even more prominent. However, to achieve convergent HEOM results at a lower T, a higher truncation level L is required, which is numerically too demanding with the present computational resources at our disposal. At $T > \Delta$, the Kondo resonance is completely destroyed. The QD system is in its linear response regime, and thus the real-time current becomes synchronized with the voltage; see Fig. 3(b).

The hysteresis feature may also exist for a noninteracting QD, provided that a single-electron level leads to the significant reduction of conductance versus bias voltage. In general, the Kondo resonance is associated with a much sharper spectral peak since $T_K \ll \Delta$, and hence a Kondo QD requires a much lower voltage for the emergence of hysteresis behavior [63]. Moreover, the hysteresis due to Kondo correlations is easily distinguished from that due to single-electron resonance by applying a gate voltage to the QD. A single-electron resonance is sensitively modulated by the gate voltage, and its corresponding hysteresis feature is greatly suppressed upon variation of ϵ_d [63]. In contrast, the Kondo resonance is always pinned to the lead chemical potential. Figure 4 shows the ac I-V curves for QDs of various ϵ_d. The electron-hole symmetry is broken at $U \neq -2\epsilon_d$, and transient charging occurs. To obtain the net conduction current, the left- and right-lead currents are symmetrized to exclude the displacement component [5]. Clearly, the Kondo-resonance-induced hysteresis behavior is continually preserved with ϵ_d shifted by as much as 4Δ. This accentuates the robustness of Kondo memory effects.

To conclude, we have demonstrated the presence of Kondo-resonance-induced memory effects in real-time electronic dynamics of strongly correlated QDs, which may be observed in experiments. The predicted hysteresis line shape and self-crossing features of the ac I-V characteristics highlight the remarkable interplay between quantum coherence and Kondo correlations. These effects may lead to novel applications of the Kondo QDs, ranging from machine learning [74] to massively parallel computation and information processing [75].

The support from the NSF of China (Grants No. 21103157, No. 21233007, and No. 21033008) (X. Z. and Y. J. Y.), the Fundamental Research Funds for Central Universities (Grants No. 2340000034 and No. 2340000025) (X. Z.), the Strategic Priority Research Program (B) of the CAS (Grant No. XDB01020000), and the Hong Kong UGC (AoE/P-04/08-2) and RGC

(No. 605012) (Y. J. Y.), is gratefully acknowledged. M. D. acknowledges support from the NSF Grant No. DMR-0802830 and the Center for Magnetic Recording Research at UCSD.

[1] Y. V. Pershin and M. Di Ventra, Adv. Phys. **60**, 145 (2011).
[2] J. J. Yang, D. B. Strukov, and D. R. Stewart, Nat. Nanotechnol. **8**, 13 (2013).
[3] M. Di Ventra, Y. V. Pershin, and L. O. Chua, Proc. IEEE **97**, 1717 (2009).
[4] T. Miyamachi, M. Gruber, V. Davesne, M. Bowen, S. Boukari, L. Joly, F. Scheurer, G. Rogez, T. K. Yamada, P. Ohresser, E. Beaurepaire, and W. Wulfhekel, Nat. Commun. **3**, 938 (2012).
[5] C. Timm and M. Di Ventra, Phys. Rev. B **86**, 104427 (2012).
[6] D. B. Strukov, G. S. Snider, D. R. Stewart, and R. S. Williams, Nature (London) **453**, 80 (2008).
[7] Z.-J. Liu, J.-Y. Gan, and T.-R. Yew, Appl. Phys. Lett. **100**, 153503 (2012).
[8] T. H. Kim, E. Y. Jang, N. J. Lee, D. J. Choi, K.-J. Lee, J.-t. Jang, J.-s. Choi, S. H. Moon, and J. Cheon, Nano Lett. **9**, 2229 (2009).
[9] D. J. Kim and Z. Fisk, Appl. Phys. Lett. **101**, 013505 (2012).
[10] D. Loss and D. P. DiVincenzo, Phys. Rev. A **57**, 120 (1998).
[11] A. Imamoğlu, D. D. Awschalom, G. Burkard, D. P. DiVincenzo, D. Loss, M. Sherwin, and A. Small, Phys. Rev. Lett. **83**, 4204 (1999).
[12] L. I. Glazman and M. E. Raikh, JETP Lett. **47**, 452 (1988), http://www.jetpletters.ac.ru/ps/1095/article_16538.shtml.
[13] T. K. Ng and P. A. Lee, Phys. Rev. Lett. **61**, 1768 (1988).
[14] Y. Meir, N. S. Wingreen, and P. A. Lee, Phys. Rev. Lett. **70**, 2601 (1993).
[15] D. Goldhaber-Gordon, H. Shtrikman, D. Mahalu, D. Abusch-Magder, U. Meirav, and M. A. Kastner, Nature (London) **391**, 156 (1998).
[16] P. W. Anderson, Phys. Rev. **124**, 41 (1961).
[17] S. Hershfield, J. H. Davies, and J. W. Wilkins, Phys. Rev. Lett. **67**, 3720 (1991).
[18] Y. Goldin and Y. Avishai, Phys. Rev. Lett. **81**, 5394 (1998).
[19] P. Nordlander, M. Pustilnik, Y. Meir, N. S. Wingreen, and D. C. Langreth, Phys. Rev. Lett. **83**, 808 (1999).
[20] P. Coleman, C. Hooley, and O. Parcollet, Phys. Rev. Lett. **86**, 4088 (2001).
[21] A. Rosch, J. Kroha, and P. Wölfle, Phys. Rev. Lett. **87**, 156802 (2001).
[22] J. R. Petta and D. C. Ralph, Phys. Rev. Lett. **89**, 156802 (2002).
[23] M. Plihal, D. C. Langreth, and P. Nordlander, Phys. Rev. B **71**, 165321 (2005).
[24] J. Eckel, F. Heidrich-Meisner, S. G. Jakobs, M. Thorwart, M. Pletyukhov, and R. Egger, New J. Phys. **12**, 043042 (2010).
[25] M. A. Cazalilla and J. B. Marston, Phys. Rev. Lett. **88**, 256403 (2002).
[26] H. G. Luo, T. Xiang, and X. Q. Wang, Phys. Rev. Lett. **91**, 049701 (2003).
[27] M. A. Cazalilla and J. B. Marston, Phys. Rev. Lett. **91**, 049702 (2003).
[28] S. R. White and A. E. Feiguin, Phys. Rev. Lett. **93**, 076401 (2004).
[29] A. J. Daley, C. Kollath, U. Schollwöck, and G. Vidal, J. Stat. Mech. 04 (2004) P04005.
[30] F. B. Anders and A. Schiller, Phys. Rev. Lett. **95**, 196801 (2005).
[31] K. A. Al-Hassanieh, A. E. Feiguin, J. A. Riera, C. A. Büsser, and E. Dagotto, Phys. Rev. B **73**, 195304 (2006).
[32] R. Gezzi, T. Pruschke, and V. Meden, Phys. Rev. B **75**, 045324 (2007).
[33] S. G. Jakobs, V. Meden, and H. Schoeller, Phys. Rev. Lett. **99**, 150603 (2007).
[34] E. Boulat, H. Saleur, and P. Schmitteckert, Phys. Rev. Lett. **101**, 140601 (2008).
[35] L. G. G. V. Dias da Silva, F. Heidrich-Meisner, A. E. Feiguin, C. A. Büsser, G. B. Martins, E. V. Anda, and E. Dagotto, Phys. Rev. B **78**, 195317 (2008).
[36] F. Heidrich-Meisner, A. E. Feiguin, and E. Dagotto, Phys. Rev. B **79**, 235336 (2009).
[37] C. H. Mak and R. Egger, J. Chem. Phys. **110**, 12 (1999).
[38] R. Egger, L. Mühlbacher, and C. H. Mak, Phys. Rev. E **61**, 5961 (2000).
[39] J. E. Han and R. J. Heary, Phys. Rev. Lett. **99**, 236808 (2007).
[40] P. Werner, T. Oka, and A. J. Millis, Phys. Rev. B **79**, 035320 (2009).
[41] M. Schiró and M. Fabrizio, Phys. Rev. B **79**, 153302 (2009).
[42] P. Werner, T. Oka, M. Eckstein, and A. J. Millis, Phys. Rev. B **81**, 035108 (2010).
[43] G. Cohen and E. Rabani, Phys. Rev. B **84**, 075150 (2011).
[44] G. Cohen, E. Gull, D. R. Reichman, A. J. Millis, and E. Rabani, Phys. Rev. B **87**, 195108 (2013).
[45] S. Weiss, J. Eckel, M. Thorwart, and R. Egger, Phys. Rev. B **77**, 195316 (2008).
[46] S. Weiss, J. Eckel, M. Thorwart, and R. Egger, Phys. Rev. B **79**, 249901(E) (2009).
[47] P. Myöhänen, A. Stan, G. Stefanucci, and R. van Leeuwen, Europhys. Lett. **84**, 67 001 (2008).
[48] K. S. Thygesen and A. Rubio, Phys. Rev. B **77**, 115333 (2008).
[49] S. Kurth, G. Stefanucci, E. Khosravi, C. Verdozzi, and E. K. U. Gross, Phys. Rev. Lett. **104**, 236801 (2010).
[50] P. Cui, X. Q. Li, J. S. Shao, and Y. J. Yan, Phys. Lett. A **357**, 449 (2006).
[51] X. Q. Li and Y. J. Yan, Phys. Rev. B **75**, 075114 (2007).
[52] J. N. Pedersen and A. Wacker, Phys. Rev. B **72**, 195330 (2005).
[53] J. S. Jin, X. Zheng, and Y. J. Yan, J. Chem. Phys. **128**, 234703 (2008).
[54] X. Zheng, R. Xu, J. Xu, J. Jin, J. Hu, and Y. J. Yan, Prog. Chem. **24**, 1129 (2012), http://www.progchem.ac.cn/EN/abstract/abstract10858.shtml.
[55] Z. H. Li, N. H. Tong, X. Zheng, D. Hou, J. H. Wei, J. Hu, and Y. J. Yan, Phys. Rev. Lett. **109**, 266403 (2012).
[56] X. Zheng, J. S. Jin, and Y. J. Yan, J. Chem. Phys. **129**, 184112 (2008).
[57] X. Zheng, J. Y. Luo, J. S. Jin, and Y. J. Yan, J. Chem. Phys. **130**, 124508 (2009).

[58] S. K. Wang, X. Zheng, J. S. Jin, and Y. J. Yan, Phys. Rev. B **88**, 035129 (2013).
[59] X. Zheng, J. S. Jin, and Y. J. Yan, New J. Phys. **10**, 093016 (2008).
[60] X. Zheng, J. S. Jin, S. Welack, M. Luo, and Y. J. Yan, J. Chem. Phys. **130**, 164708 (2009).
[61] G. Stefanucci and C.-O. Almbladh, Phys. Rev. B **69**, 195318 (2004).
[62] J. Maciejko, J. Wang, and H. Guo, Phys. Rev. B **74**, 085324 (2006).
[63] See the Supplemental Material at http://link.aps.org/supplemental/10.1103/PhysRevLett.111.086601 for more details about the HEOM approach and calculations.
[64] J. Gabelli, G. Fève, J.-M. Berroir, B. Placais, A. Cavanna, B. Etienne, Y. Jin, and D. C. Glattli, Science **313**, 499 (2006).
[65] G. Fève, A. Mahé, J.-M. Berroir, T. Kontos, B. Plaçais, D. C. Glattli, A. Cavanna, B. Etienne, and Y. Jin, Science **316**, 1169 (2007).
[66] G. Cao, H.-O. Li, T. Tu, L. Wang, C. Zhou, M. Xiao, G.-C. Guo, H.-W. Jiang, and G.-P. Guo, Nat. Commun. **4**, 1401 (2013).
[67] C.-Y. Yam, Y. Mo, F. Wang, X. Li, G. H. Chen, X. Zheng, Y. Matsuda, J. Tahir-Kheli, and W. A. Goddard, III, Nanotechnology **19**, 495203 (2008).
[68] Y. Mo, X. Zheng, G. H. Chen, and Y. J. Yan, J. Phys. Condens. Matter **21**, 355301 (2009).
[69] S. Wen, S. K. Koo, C. Y. Yam, X. Zheng, Y. J. Yan, Z. M. Su, K. N. Fan, L. Cao, W. P. Wang, and G. H. Chen, J. Phys. Chem. B **115**, 5519 (2011).
[70] J. Wang, B. Wang, and H. Guo, Phys. Rev. B **75**, 155336 (2007).
[71] A. Kaminski, Y. V. Nazarov, and L. I. Glazman, Phys. Rev. Lett. **83**, 384 (1999).
[72] A. Kaminski, Y. V. Nazarov, and L. I. Glazman, Phys. Rev. B **62**, 8154 (2000).
[73] G. Z. Cohen, Y. V. Pershin, and M. Di Ventra, Appl. Phys. Lett. **100**, 133109 (2012).
[74] Y. V. Pershin, S. La Fontaine, and M. Di Ventra, Phys. Rev. E **80**, 021926 (2009).
[75] Y. V. Pershin and M. Di Ventra, Phys. Rev. E **84**, 046703 (2011).